J|A|C|S ARTICLES

Published on Web 06/18/2010

Electrified Selective "Sponges" Made of Au Nanoparticles

Marco Frasconi, Ran Tel-Vered, Michael Riskin, and Itamar Willner*

Institute of Chemistry, The Hebrew University of Jerusalem, Jerusalem 91904, Israel

Received March 14, 2010; E-mail: willnea@vms.huji.ac.il

Abstract: Imprinted Au nanoparticle (NP) composites are assembled on Au surfaces by the electropolymerization of thioaniline-functionalized Au NPs in the presence of the imprint molecules, picric acid (**1**), *N,N′*-dimethyl-4,4′-bipyridinium (**2**), and *N,N′*-dimethylbipyridinium-4,4′-ethylene dichloride (**3**). The existence of π-donor−acceptor complexes between the substrates (**1**−**3**) and the π-donor thioaniline units associated with the Au NPs or the π-donor bis-aniline bridges cross-linking the Au NPs on the electrode surfaces led to the formation of the imprinted sites. Upon elimination of the electron acceptors (**1**−**3**) from the Au NP matrices, molecular contours for the selective binding of the respective substrates are generated. The bis-aniline bridges linking the Au NPs in the composite exhibit quasireversible redox properties. At $E <$ 0.12 V vs Ag quasireference electrode (QRE), the bridges exist in the reduced bis-aniline, π-donor state, whereas at $E >$ 0.12 V vs Ag QRE, the bridging units exist in the quinoid, π-acceptor state. As a result, the potential-induced uptake and release of any of the π-acceptor substrates **1**−**3** is accomplished. While at $E <$ 0.12 V, the π-acceptor substrates bind to the Au NP matrices through π-donor−acceptor interactions, at $E >$ 0.12 V, the bound substrates are released from the matrices, due to transformation of the bridging units to the quinoid π-acceptor state, which lacks binding affinity for the substrates. The binding and release of the substrates **1**−**3** to and from the Au NP composites are followed by surface plasmon resonance (SPR) spectroscopy, and the quantitative assay of the uptake and release is monitored by the extent of fluorescence quenching of the solution-soluble fluorescent labels, *meso*-tetramethyl pyridinium porphyrin ($TMPyP^{4+}$) or Zn(II)−*meso*-tetraphenylsulfonatoporphyrin (Zn−$TPPS^{4-}$). The electrostimulated functions of the Au NP "sponges" are controlled by several means: (i) Imprinting of the molecular contours for **1**−**3** in the Au NP composites generates high-affinity binding sites for the imprinted substrates. This leads to higher contents of the bound substrates at the Au NP sponges, as compared to the nonimprinted Au NP composites, and to an impressive selectivity in the association of the imprinted substrates. (ii) The binding capacity of the Au NP composites is substantially improved by the electrosynthesis of the matrices on a rough Pt black support bound to the base Au electrode.

Introduction

The controlled uptake and release of ions or molecular substrates to and from solid matrices has important implications in chromatographic separations, controlled release of substances, and removal of pollutants. Two important elements must be considered upon developing uptake/release systems, and these include (i) the development of specific supports for the uptake/release of the substrate and (ii) the design of matrices that respond to external signals stimulating the uptake and release processes. Molecularly imprinted polymers provide versatile matrices for the selective uptake of molecular or ionic substrates, and these were extensively used for chromatographic separation, sensing, and slow release of materials.[1−4] Particularly, imprinted polymers were used for drug delivery[5] and for the removal of pollutants.[6] Stimuli-responsive polymers were developed[7] and different external signals, such as temperature,[8] pH,[9] or light[10] were used to trigger phase transitions of polymers that stimulate the uptake or release of the substrates from the polymeric matrices. Specifically, molecularly imprinted polymers were suggested as selective engineered materials for stimuli-controlled drug delivery and other biomedical applications.[11] Recently, silica mesoporous nanoparticles were used as containers for the

(1) (a) Ye, L.; Mosbach, K. *Chem. Mater.* **2008**, *20*, 859–869. (b) Wulff, G. *Chem. Rev.* **2002**, *102*, 1–28. (c) Severin, K. In *Molecularly Imprinted Materials. Science and Technology*; Yan, M., Ramström, O., Eds.; Marcel Dekker: New York, 2005; pp 619−683. (d) Alexander, C.; Andersson, H. S.; Andersson, L. I.; Ansell, R. J.; Kirsch, N.; Nicholls, I. A.; O'Mahony, J.; Whitcombe, M. J. *J. Mol. Recognit.* **2006**, *19*, 106–180.

(2) (a) Yu, Y.; Ye, L.; Haupt, K.; Mosbach, K. *Angew. Chem., Int. Ed.* **2002**, *41*, 4459–4463. (b) Cutivet, A.; Schembri, C.; Kovensky, J.; Haupt, K. *J. Am. Chem. Soc.* **2009**, *131*, 14699–14702. (c) Liu, J. Q.; Wulff, G. *J. Am. Chem. Soc.* **2008**, *130*, 8044–8054. (d) Wulff, G. In *Templated Organic Synthesis*; Diederich, F., Stang, P. J., Eds.; Wiley-VCH: Weinheim, 2000; pp 39−73.

(3) (a) Haupt, K.; Mosbach, K. *Chem. Rev.* **2000**, *100*, 2495–2504. (b) Ye, L.; Haupt, K. *Anal. Bioanal. Chem.* **2004**, *378*, 1887–1897. (c) Benito-Pena, E.; Moreno-Bondi, M. C.; Aparicio, S.; Orellana, G.; Cederfur, J.; Kempe, M. *Anal. Chem.* **2006**, *78*, 2019–2027.

(4) (a) Mullett, W. M.; Martin, P.; Pawliszyn, J. *Anal. Chem.* **2001**, *73*, 2383–2389. (c) Caro, E.; Marce', R. M.; Borrull, F.; Cormack, P. A. G.; Sherrington, D. C. *Trends Anal. Chem.* **2006**, *25*, 143–154. (b) Dias, A. C. B.; Figueiredo, E. C.; Grassi, V.; Zagatto, E. A. G.; Arruda, M. A. Z. *Talanta* **2008**, *76*, 988–996.

(5) (a) Sellergren, B.; Allender, C. J. *Adv. Drug Delivery Rev.* **2005**, *57*, 1733–1741. (b) Cunliffe, D.; Kirby, A.; Alexander, C. *Adv. Drug Delivery Rev.* **2005**, *57*, 1836–11853.

(6) (a) Meng, Z.; Chen, W.; Mulchandani, A. *Environ. Sci. Technol.* **2005**, *39*, 8958–8962. (b) Rao, T. P.; Daniel, S.; Gladis, J. M. *Trends Anal. Chem.* **2004**, *23*, 28–35.

controlled release of substrates.[12] The respective substrates were entrapped in the pores of the nanoparticles and locked by molecular lids. The mechanized opening of the pores by external stimuli, such as pH,[13] light,[14] redox activity,[15] or enzymatic reactions[16] resulted in the release of the entrapped substrates. Most of these nanoscale containers are, however, single-cycle-release systems operating as diffusional components in solutions. Here we report on the electrochemical polymerization of imprinted Au nanoparticle matrices on electrode surfaces and their use as electrified "sponges" for the reversible uptake and release of molecular substrates.

The imprinting of Au nanoparticle (NP) composites assembled on Au electrodes was recently demonstrated by the electropolymerization of thioaniline-functionalized Au NPs on thioaniline-modified Au surfaces in the presence of molecular analogs to explosive substrates (TNT or RDX). The resulting matrices were used for the specific sensing of the explosives.[17,18] The shifts of the surface plasmon resonance (SPR) curves upon the binding of the explosives to the imprinted sites were amplified by the coupling between the localized Au NPs plasmon and the surface plasmon wave, a process that was affected by the dielectric constant changes occurring upon the binding of the substrates to the recognition sites.

Results and Discussion

The electrochemical synthesis of the Au NP sponge on electrode surfaces is depicted in Scheme 1. Thioaniline-functionalized Au NPs, that are also modified with mercaptoethanesulfonic acid for enhanced stability (diameter ca. 4.0 nm), were electropolymerized on a thioaniline-modified surface in the presence of picric acid (**1**) or *N*,*N*′-dimethyl-4,4′-bipyridinium dichloride (methyl viologen, MV^{2+}) (**2**) as imprint substrates. The π-donor−acceptor complexes between the electrochemically synthesized bis-aniline bridging units and **1** or **2** provide the driving force for the formation of the molecular contours of the imprinted substrates in the Au NP composite. The imprinted substrates **1** or **2** were then eliminated from the composite by a rinsing process (the removal of the imprinted substrates from the **1**- and **2**-imprinted matrices was followed by SPR spectroscopy; see Figures S1 and S2 of the Supporting Information, respectively). Similarly, by the electropolymerization of the functionalized Au NPs in the absence of **1** or **2**, the nonimprinted composite was synthesized on the Au surface and then treated under similar conditions applied to rinse the imprinted matrix. The bis-aniline bridging units are electroactive and exhibit a quasireversible redox wave at $E^0 = 0.12$ V vs Ag quasireference wire electrode (QRE) at pH = 7.2 (see Figure S3, Supporting Information), and thus, at $E < 0.12$ V vs Ag QRE, the bridging units exist in their reduced state and exhibit π-donor properties, whereas at $E > 0.12$ V, the bridges exist in the quinoid state that reveals π-acceptor properties. Thus, the π-acceptor substrates **1** or **2** would bind to the imprinted sites at potentials lower than $E = 0.12$ V, where the bridging units act as π-donor sites, while the oxidation of the bridging units ($E > 0.12$ V) and their transformation to the quinoid π-acceptor state would release the substrates from the Au NP matrices.

Figure 1A shows the reflectance changes of the picric acid-imprinted surface upon its interaction with different concentrations of **1**, and the resulting calibration curve is shown in Figure 1B, curve a. For comparison, the calibration curve corresponding to the association of picric acid to the nonimprinted Au NP composite is shown in Figure 1B, curve b. Evidently, the association of **1** to the **1**-imprinted Au NP composite is significantly higher than to the nonimprinted Au NP matrix, consistent with the formation of imprinted molecular sites that reveal high affinities for **1**. The calibration curve corresponding to the binding of picric acid to the imprinted sites levels off at a bulk concentration of **1** of 1×10^{-11} M, implying that at this concentration the imprinted sites are saturated. Assuming a Langmuir-type binding of **1** to the imprinted sites, the association constant of picric acid to the imprinted sites was derived to be $K_a = 3.9 \times 10^{12}$ M^{-1} (see Figure S4, Supporting Information). Figure 2 depicts the reversible electrified activities of the Au NP sponge. The Au NP composite associated with

(7) (a) Alexander, C.; Shakesheff, K. M. *Adv. Mater.* **2006**, *18*, 3321–3328. (b) Tokarev, I.; Minko, S. *Adv. Mater.* **2009**, *21*, 241–247. (c) Shneider, H.-J.; Strongin, R. M. *Acc. Chem. Res.* **2009**, *42*, 1489–1500. (d) de las Heras Alarcón, C.; Pennadam, S.; Alexander, C. *Chem. Soc. Rev.* **2005**, *34*, 276–285. (e) Schmaljohann, D. A. *Adv. Drug Delivery Rev.* **2006**, *58*, 1655–1670. (f) Jeong, B.; Gutowska, A. *Trends Biotechnol.* **2002**, *20*, 305–311. (g) Gupta, P.; Vermani, K.; Garg, S. *Drug Discov. Today* **2002**, *10*, 569–579.

(8) (a) Lutz, J.-F.; Akdemir, O.; Hoth, A. *J. Am. Chem. Soc.* **2006**, *128*, 13046–13047. (b) Pasparakis, G.; Cockayne, A.; Alexander, C. *J. Am. Chem. Soc.* **2007**, *129*, 11014–11015. (c) Riskin, M.; Tel-Vered, R.; Willner, I. *Adv. Funct. Mater.* **2009**, *19*, 2474–3480. (d) Zhu, Z.; Sukhishvili, S. A. *ACS Nano* **2009**, *3*, 3595–3605.

(9) (a) Kanakijo, Y.; Naganawa, R.; Tao, H. *Angew. Chem., Int. Ed.* **2003**, *42*, 3014–3016. (b) Kozlovskaya, V.; Kharlampieva, E.; Khanal, B. P.; Manna, P.; Zubarev, E. R.; Tsukruk, V. V. *Chem. Mater.* **2008**, *20*, 7474–7485. (c) Lee, D.; Nolte, A. J.; Kunz, A. L.; Rubner, M. F.; Cohen, R. E. *J. Am. Chem. Soc.* **2006**, *128*, 8521–8529. (d) Park, M.-K.; Deng, S.; Advincula, R. C. *J. Am. Chem. Soc.* **2004**, *126*, 13723–13731.

(10) (a) Gorelikov, I.; Field, L. M.; Kumacheva, E. *J. Am. Chem. Soc.* **2004**, *126*, 15938–15939. (b) Minoura, N.; Idei, K.; Rachkov, A.; Choi, Y.-W.; Ogiso, M.; Matsuda, K. *Macromolecules* **2004**, *37*, 9571–9576. (c) Gong, C.; Lam., M. H.-W.; Yu, H. *Adv. Funct. Mater.* **2006**, *16*, 1759–1767. (d) Lee, H.; Wu, W.; Oh, J. K.; Mueller, L.; Sherwood, G.; Peteanu, L.; Kowalewski, T.; Matyjaszewski, K. *Angew. Chem., Int. Ed.* **2007**, *46*, 2453–2457.

(11) (a) Puoci, F.; Iemma, F.; Picci, N. *Curr. Drug Deliv.* **2008**, *5*, 85–96. (b) Watanabe, M.; Akahoshi, T.; Tabata, Y.; Nakayama, D. *J. Am. Chem. Soc.* **1998**, *120*, 5577–5578. (c) Miyata, T.; Jige, M.; Nakaminami, T.; Uragami, T. *Proc. Natl. Acad. Sci. U.S.A.* **2006**, *103*, 51190–51193.

(12) (a) Cotí, K. K.; Belowich, M. E.; Liong, M.; Ambrogio, M. W.; Lau, Y. A.; Khatib, H. A.; Zink, J. I.; Khashab, N. M.; Stoddart, J. F. *Nanoscale* **2009**, *1*, 16–39. (b) Vallet-Regí, M.; Balas, F.; Arcos, D. *Angew. Chem., Int. Ed.* **2007**, *46*, 7548–7558. (c) Slowing, I. I.; Trewyn, B. G.; Giri, S.; Lin, V. S.-Y. *Adv. Funct. Mater.* **2007**, *17*, 1225–1236.

(13) (a) Khashab, N. M.; Belowich, M. E.; Trabolsi, A.; Friedman, D. C.; Valente, C.; Lau, Y.; Khatib, H. A.; Zink, J. I.; Stoddart, J. F. *Chem. Commun.* **2009**, 5371–5373. (b) Hong, C.-Y.; Li, X.; Pan, C.-Y. *J. Mater. Chem.* **2009**, *19*, 5155–5160. (c) Park, C.; Oh, K.; Lee, S. C.; Kim, C. *Angew. Chem., Int. Ed.* **2007**, *46*, 1455–1457. (d) Du, L.; Liao, S.; Khatib, H. A.; Stoddart, J. F.; Zink, J. I. *J. Am. Chem. Soc.* **2009**, *131*, 15136–152142. (e) Casasús, R.; Climent, E.; Marcos, M. D.; Martínez-Máñez, R.; Sancenón, F.; Soto, J.; Amorós, P.; Cano, J.; Ruiz, E. *J. Am. Chem. Soc.* **2008**, *130*, 1903–1917.

(14) (a) Angelos, S.; Yang, Y.-W.; Khashab, N. M.; Stoddart, F. J.; Zink, J. I. *J. Am. Chem. Soc.* **2009**, *131*, 11344–11346. (b) Zhu, Y.; Fujiwara, M. *Angew. Chem., Int. Ed.* **2007**, *46*, 2241–2244. (c) Lu, J.; Choi, E.; Tamanoi, F.; Zink, J. I. *Small* **2008**, *4*, 421–426. (d) Park, C.; Lee, K.; Kim, C. *Angew. Chem., Int. Ed.* **2009**, *48*, 1275–1278.

(15) (a) Klajn, R.; Olson, M. A.; Wesson, P. J.; Fang, L.; Coskun, A.; Trabolsi, A.; Soh, S.; Stoddart, J. F.; Grzybowski, B. A. *Nat. Chem.* **2009**, *1*, 733–738. (b) Khashab, N. M.; Trabolsi, A.; Lau, Y. A.; Ambrogio, M. W.; Friedman, D. C.; Khatib, H. A.; Zink, J. I.; Stoddart, J. F. *Eur. J. Org. Chem.* **2009**, 1669–1673.

(16) (a) Park, C.; Kim, H.; Kim, S.; Kim, C. *J. Am. Chem. Soc.* **2009**, *131*, 16614–16615. (b) Schossbauer, A.; Kecht, J.; Bein, T. *Angew. Chem., Int. Ed.* **2009**, *48*, 3092–3095.

(17) Riskin, M.; Tel-Vered, R.; Lioubashevski, O.; Willner, I. *J. Am. Chem. Soc.* **2009**, *131*, 7368–7378.

(18) Riskin, M.; Tel-Vered, R.; Willner, I. *Adv. Mater.* **2010**, *22*, 1387–1391.

Scheme 1. Schematic Presentation of the Electropolymerization of the Bis-Aniline-Cross-Linked Au NP Composite and the Imprinting of the π-Acceptor Molecules Picric Acid (**1**), *N,N′*-Dimethyl-4,4′-bipyridinium (**2**), and *N,N′*-Dimethylbipyridinium-4,4′-ethylene Dichloride (**3**)

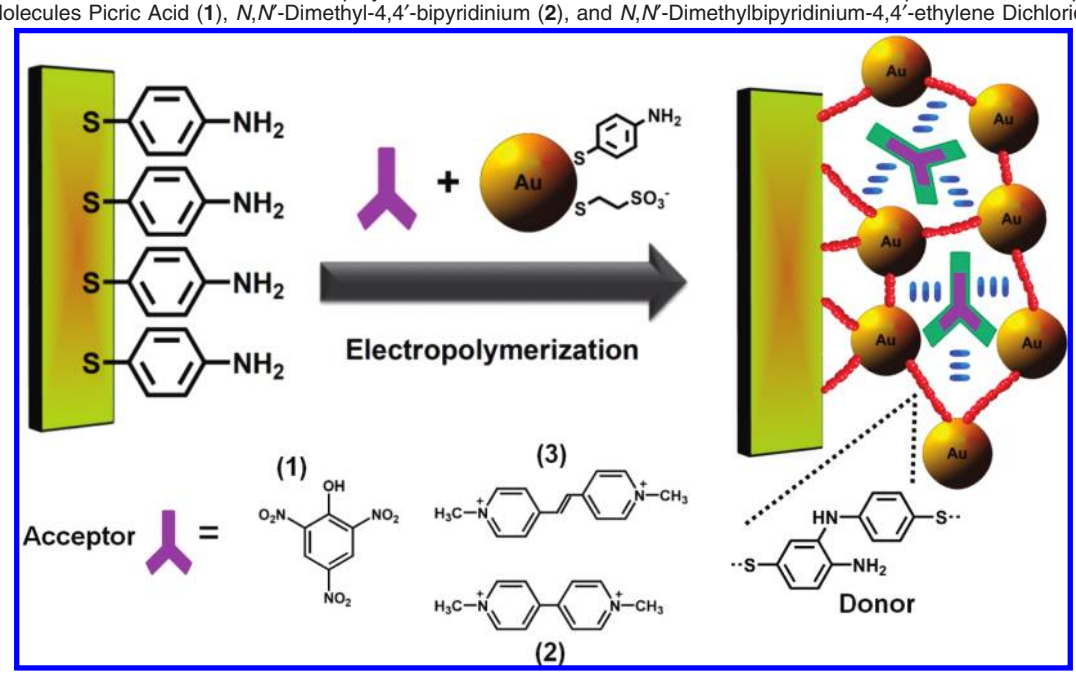

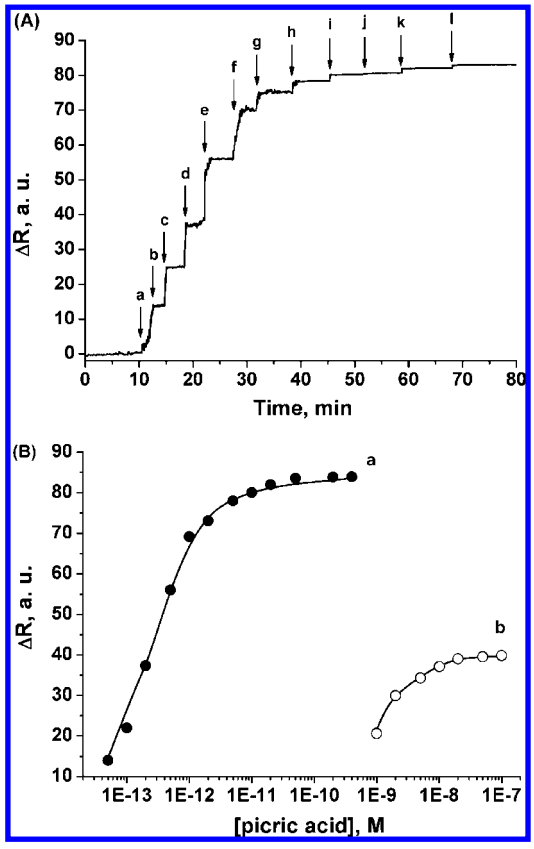

Figure 1. (A) Sensogram corresponding to the changes in the reflectance intensities, at $\theta = 62.0°$, by the picric acid-imprinted bis-aniline-cross-linked Au NP composite, upon addition of variable concentrations of picric acid: (a) 50 fM, (b) 100 fM, (c) 200 fM, (d) 500 fM, (e) 1 pM, (f) 2 pM, (g) 5 pM (h) 10 pM, (i) 20 pM, (j) 50 pM, (k) 200 pM, (l) 400 pM. Arrows indicate the time of addition of picric acid. (B) Calibration curves corresponding to the reflectance changes at different concentrations of added picric acid on (a) the picric acid-imprinted bis-aniline-cross-linked Au NP composite and (b) the nonimprinted bis-aniline-cross-linked Au NP composite. All measurements were performed in a 0.1 M HEPES buffer solution (pH = 7.2).

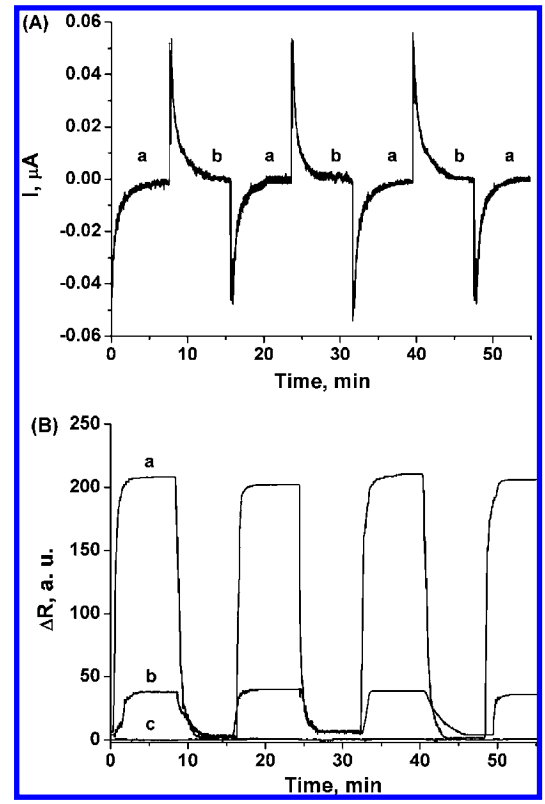

Figure 2. (A) Current transient of the picric acid-imprinted bis-aniline-cross-linked Au NP composite-modified Au electrode upon the application of cyclic reduction potential ($E = -0.3$ V vs Ag QRE, time intervals a) and oxidation potential ($E = 0.4$ V vs Ag QRE, time intervals b). Potential steps were applied in a 0.1 M HEPES buffer solution (pH = 7.2). (B) Reflectance changes corresponding to the cyclic electrostimulated uptake and release of picric acid, 160 pM, by (a) the picric acid-imprinted bis-aniline-cross-linked Au NP composite-modified Au electrode and (b) the nonimprinted bis-aniline-cross-linked Au NP composite. Curve c corresponds to the cyclic application of the reduction, $E = -0.3$ V, and oxidation, $E = 0.4$ V, potentials on a thioaniline monolayer-modified Au surface.

Scheme 2. Photonic Imaging of the Electro-Stimulated Uptake and Release of π-Acceptor Molecules Using the Imprinted Bis-Aniline-Cross-Linked Au NP Composite

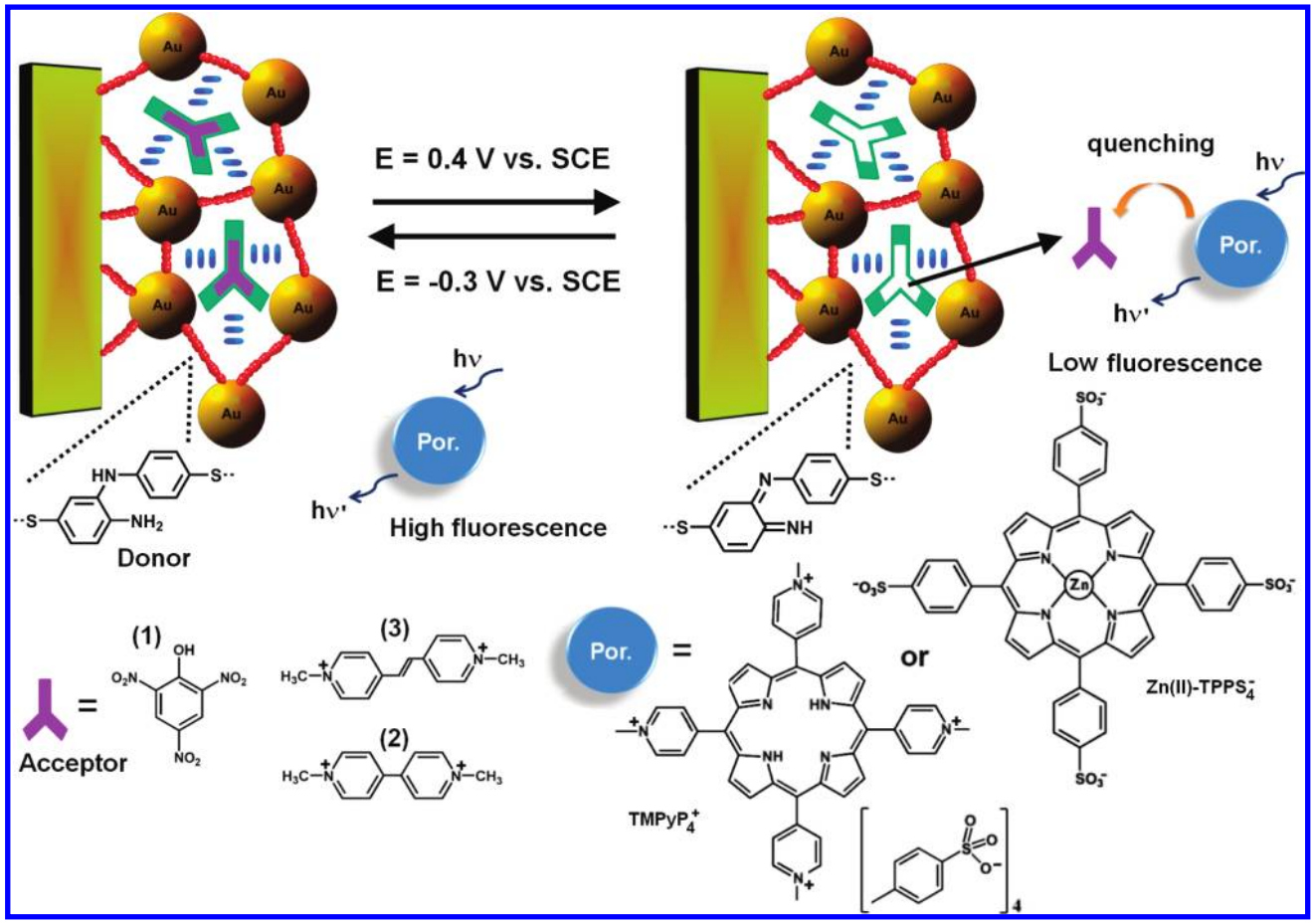

the Au surface was subjected to a series of oxidative and reductive potential pulses that oxidize the bis-aniline bridges to the quinoid acceptor state and reduce the bridges to the bis-aniline π-donor state, respectively (Figure 2A). The concomitant SPR reflectance changes of the **1**-imprinted Au NP composite-modified electrode, subjected to the series of applied potential cycles, are depicted in Figure 2B, curve a. For comparison, the SPR reflectance changes observed upon the application of the potential cycles on the nonimprinted Au NP-modified electrode are shown in curve b, whereas no reflectance changes were observed on a thioaniline-monolayer-modified Au surface (curve c). The reflectance changes in curve a are consistent with the uptake of picric acid by the Au NP composite and its release. When the composite is subjected to the negative potential of $E = -0.3$ V (time intervals a, Figure 2A), the reflectance reaches a high value, consistent with the uptake of **1** into the Au NP composite (Figure 2B, curve a). At time intervals b (Figure 2A), the surface modified with the Au NP composite was subjected to the positive potential of $E = 0.4$ V. At this potential the bis-aniline π-donor bridges are transformed to the quinoid π-acceptor configuration. The removal of the stabilized π-donor−acceptor interaction results in the release of **1** from the Au NP sponge, as evident by the decrease in the reflectance values (Figure 2B, curve a). By the cyclic application of the negative and positive potentials, the reversible uptake of **1** into the composite, and its release from the aggregated Au NPs, are demonstrated. Furthermore, it is evident that the high affinity of **1** to the imprinted sites allows the uptake and release of a substantially higher amount of **1** as compared to the nonimprinted Au NP composite (cf. curves a vs b, Figure 2B).

The electrically driven uptake and release of **1** by the Au NP sponge was further examined by using *meso*-tetramethylpyridinium porphyrin ($TMPyP^{4+}$) as a fluorescent label in solution (Scheme 2). Picric acid quenches the fluorescence of $TMPyP^{4+}$ (Figure S5, Supporting Information), and the respective calibration curve was derived (Figure S5, inset). Figure 3A shows the fluorescence spectra of $TMPyP^{4+}$ upon the application of the negative and positive potentials on the **1**-imprinted Au NP composite in the presence of **1**. When the electrode was subjected to the negative potential ($E = -0.3$ V), a high fluorescence value of $TMPyP^{4+}$ was observed (curve a), whereas the application of the positive potential ($E = 0.4$ V) resulted in a low fluorescence value, (curve b). Control experiments indicated that the fluorescence of $TMPyP^{4+}$ is not affected by the potential changes in the absence of **1**. These observations are consistent with the uptake of **1** by the composite subjected to the negative potential, resulting in high fluorescence (decreased quenching) and lower fluorescence intensity upon oxidation of the bridging units and the release of **1**, resulting in an improved quenching of the $TMPyP^{4+}$. By the cyclic electrochemical reduction and the oxidation of the Au NPs bridging units, the fluorescence of $TMPyP^{4+}$ was reversibly switched between high and low values, consistent with the uptake and release of **1** into and from the Au NP sponge, respectively (Figure 3B). Again, minute fluorescence changes were observed upon cycling the potential on the nonimprinted

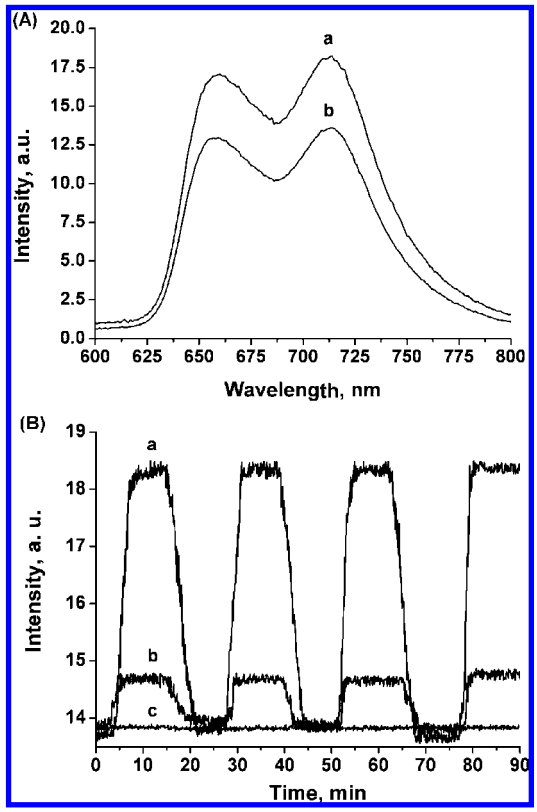

Figure 3. (A) Emission spectra measured for *meso*-tetramethylpyridinium porphyrin, $TMPyP^{4+}$, 2 nM, in a 0.1 M HEPES buffer solution (pH = 7.2) that included picric acid, 160 pM, following the application of (a) reduction potential, $E = -0.3$ V vs Ag QRE, for 10 min and (b) oxidation potential, $E = 0.4$ V vs Ag QRE, for 10 min on the picric acid-imprinted bis-aniline-cross-linked Au NP composite-modified Au electrode. (B) Switchable fluorescence intensity changes, at $\lambda = 715$ nm, corresponding to $TMPyP^{4+}$, 2 nM, in a 0.1 M HEPES buffer solution (pH = 7.2), following the cyclic electrostimulated uptake and release of picric acid by (a) the picric acid-imprinted bis-aniline-cross-linked Au NP composite-modified Au electrode and (b) the nonimprinted bis-aniline-cross-linked Au NP composite. Curve c corresponds to the cyclic application of the reduction, $E = -0.3$ V, and oxidation, $E = 0.4$ V, potentials on a thioaniline-monolayer-modified Au surface. In all the experiments the concentration of picric acid was 160 pM, and the excitation wavelength was $\lambda_{ex} = 430$ nm.

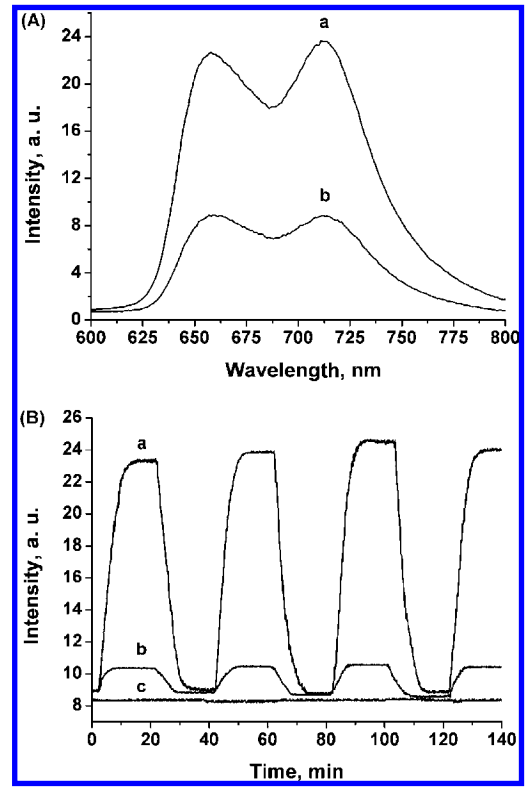

Figure 4. (A) Emission spectra corresponding to the *meso*-tetramethyl pyridinium porphyrin, $TMPyP^{4+}$, 2 nM, in a 0.1 M HEPES buffer solution (pH = 7.2) that included picric acid 360 pM, following the application of (a) reduction potential, $E = -0.3$ V vs Ag QRE, for 10 min and (b) oxidation potential, $E = 0.4$ V vs Ag QRE, for 10 min on the picric acid-imprinted bis-aniline-cross-linked Au NP composite-modified Pt black-roughened Au electrode. (B) Switchable fluorescence intensity changes, at $\lambda = 715$ nm, corresponding to $TMPyP^{4+}$, 2 nM, in a 0.1 M HEPES buffer solution (pH = 7.2), following the cyclic electrostimulated uptake and release of picric acid by (a) the picric acid-imprinted bis-aniline-cross-linked Au NP composite-modified Pt black-roughened Au electrode and (b) the nonimprinted bis-aniline-cross-linked Au NP composite on the modified Pt black-roughened Au electrode. Curve c corresponds to the cyclic application of the reduction, $E = -0.3$ V, and oxidation, $E = 0.4$ V, potentials on a thioaniline monolayer-modified Pt black-roughened Au surface. In all the experiments the concentration of picric acid was 360 pM and the excitation wavelength was $\lambda_{ex} = 430$ nm.

Au NP matrix (curve b), and no responses were observed on the thioaniline-monolayer-modified Au electrode (curve c). From the changes in the fluorescence intensities, we estimate that 5.5×10^{-14} mol·cm^{-2} of **1** was uptaken or released by the matrix upon the application of the respective potentials.

In order to enhance the uptake/release capabilities of the imprinted Au NP composite, the surface area of the support on which the Au NPs were electropolymerized was increased. Pt black was deposited on the Au surface, and the imprinted composite consisting of the bis-aniline-cross-linked Au NPs was electropolymerized on the rough Pt black support in the presence of picric acid. After the removal of the imprint molecule, the resulting functionalized electrode was characterized and used for the uptake and release of **1**. Coulometric analysis of the redox wave of the bis-aniline bridges associated with the Au NP composite revealed that the content of the π-donor sites (and thus of the Au NPs) increased by ca. 6-fold as compared to the coverage of the bis-aniline-cross-linked Au NPs linked to the base Au surface. Figure 4A shows the fluorescence intensities of the $TMPyP^{4+}$ fluorophore upon applying the reductive potential ($E = -0.3$ V) (curve a) and the oxidative potential ($E = 0.4$ V) (curve b) on the Pt black-roughened/imprinted Au NPs structure. Upon the reduction of the bridges to the π-donor bis-aniline state, high fluorescence is observed, indicating the effective uptake of **1** by the composite (less efficient quenching). Oxidation of the bridging units to the quinoid cross-linkers ($E = 0.4$ V) resulted in a low fluorescence of $TMPyP^{4+}$, implying that **1** was released from the composite, and thus, the quenching of the solution-solubilized $TMPyP^{4+}$ was intensified. Upon the cyclic application of the reductive and oxidative potentials on the electrode, the fluorescence intensities of $TMPyP^{4+}$ were reversibly cycled between low and high values (Figure 4B), demonstrating that the uptake and release of **1** into the Au NP sponge, and from it, can be reversibly stimulated. As before, the nonimprinted Au NP matrix deposited on the Pt black-roughened Au surface reveals smaller fluorescence changes (Figure 4B, curve b), implying that the imprint of molecular recognition sites in the Au NP composite is essential for the effective uptake and release of the guest substrate, picric acid. Using the calibration curve corresponding to the quenching of $TMPyP^{4+}$ by variable concentrations of **1** (Figure S5, Supporting Information) and the fluorescence intensities shown in Figure 4A, we conclude that the Au NP

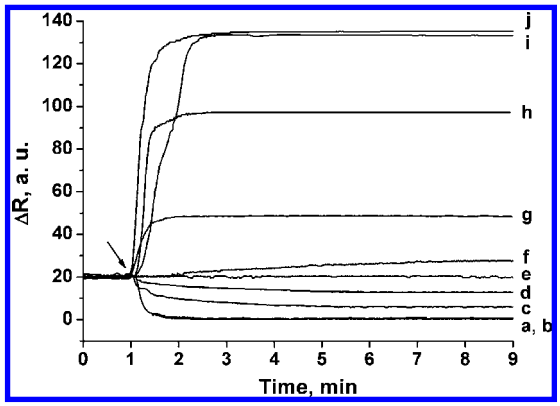

Figure 5. Time-dependent reflectance changes, at $\theta = 62.0°$, corresponding to the application of variable potential pulses on the picric acid-imprinted bis-aniline-cross-linked Au NP composite-modified Pt black-roughened Au electrode: (a) 0.5 V, (b) 0.4 V, (c) 0.3 V, (d) 0.2 V, (e) 0.1 V, (f) 0.0 V, (g) −0.1 V, (h) −0.2 V, (i) −0.3 V, (j) −0.4 V. The measurements were performed in a 0.1 M HEPES buffer solution that included picric acid, 100 fM.

composite linked to the Pt black-roughened Au surface binds and releases 2.8×10^{-13} mol·cm^{-2} of picric acid, a value that is higher than the uptake and release of **1** by the Au NP matrix electropolymerized on the base Au surface. The enhanced binding/release capacities of the Au NPs deposited on the rough Pt support correlate nicely with the increased content of Au NPs on the rough surface, as deduced from the Coulometric assay of the bis-aniline bridging units. It should be noted that the uptake and release of picric acid by the imprinted bis-aniline-cross-linked composite is selective,[17] and the imprinted matrix did not respond to the presence of 2,4-dinitrophenol or nitrophenol.

A further aspect to consider relates to the effect of the applied potential on the uptake and release of picric acid into and from the Au NP composite sponge. Figure 5 shows the time-dependent reflectance changes of the **1**-imprinted Au NP system in the presence of **1** (1×10^{-13} M). The surface was equilibrated with **1**, and at the time indicated with an arrow, the surface was subjected to the appropriate applied potential. As the potential is negatively shifted, the reflectance changes intensify, and they reach a saturation value at $E = -0.3$ V. These observations are consistent with the fact that as the potential is negatively shifted, more bis-aniline units exist in their reduced π-donor state, and thus, the binding affinity of the matrix toward **1** improves. As the potential is shifted to more positive values (curves a−d), the reflectance changes are negatively shifted as compared to the base open circuit potential reflectance level of the system (curve e). As the applied potential is positively shifted, the fraction of the bridges in the oxidized state increases, leading to a lower degree of binding of **1** to the composite. At an applied potential of $E = 0.4$ V, all bridges are in their oxidized form, resulting in the lowest value of reflectance.

The Au NP composite was further applied to follow the uptake and release of *N*,*N*′-dimethyl-4,4′-bipyridinium dichloride, MV^{2+} (**2**), into and from the Au NP sponge. The substrate **2** is a common herbicide, and thus, the experiment represents the application of the system to remove and purify the herbicide-contaminated solution. The thioaniline-functionalized Au NPs were electropolymerized on the Au surface in the presence of **2**. As the bipyridinium salt is an electron acceptor, the formation of π-donor−acceptor complexes between the bridging units and **2** is anticipated to yield the imprinted molecular contours for **2**

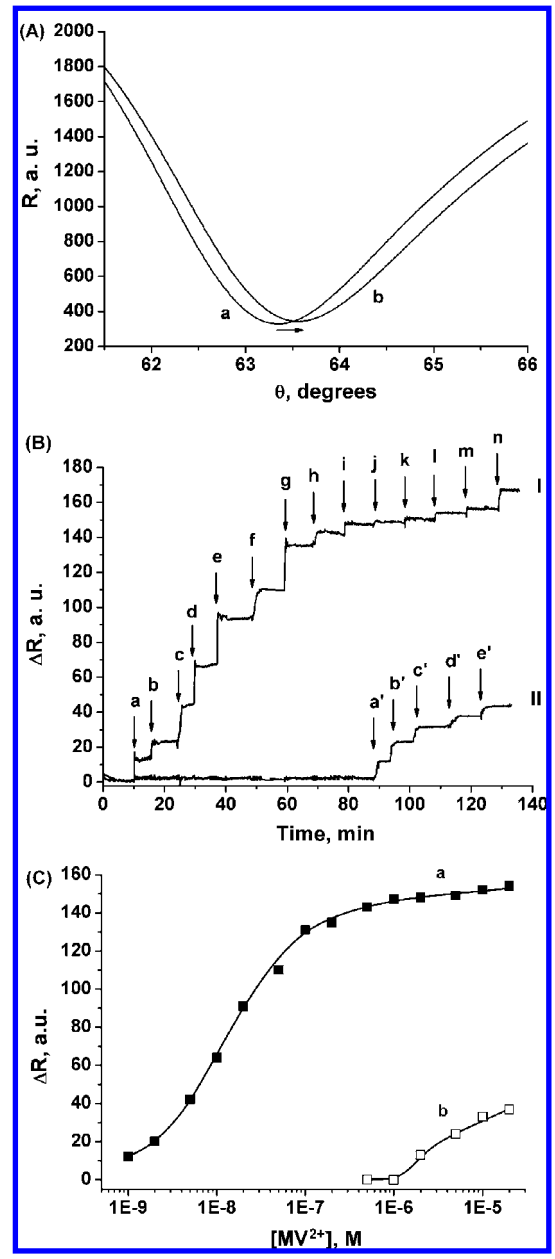

Figure 6. (A) SPR curves corresponding to the MV^{2+} (**2**)-imprinted bis-aniline-cross-linked Au NP composite-modified Au electrode (a) before, and (b) after interacting the electrode with MV^{2+}, 1 μM. (B) Sensograms corresponding to the changes in the reflectance intensities, at $\theta = 62.0°$, by (sensogram I) the MV^{2+} (**2**)-imprinted bis-aniline-cross-linked Au NP composite, upon the addition of variable concentrations of MV^{2+}: (a) 1 nM, (b) 2 nM, (c) 5 nM, (d) 10 nM, (e) 20 nM, (f) 50 nM, (g) 100 nM (h) 200 nM, (i) 500 nM, (j) 1 μM, (k) 2 μM, (l) 5 μM, (m) 10 μM, (n) 20 μM. Sensogram II: The nonimprinted bis-aniline-cross-linked Au NP composite, upon the addition of variable concentrations of MV^{2+}: (a′) 1 μM, (b′) 2 μM, (c′) 5 μM, (d′) 10 μM, (e′) 20 μM. Arrows indicate the time of addition of MV^{2+}. (C) Calibration curves corresponding to the reflectance changes at different concentrations of added MV^{2+} on (a) the MV^{2+}-imprinted bis-aniline-cross-linked Au NP composite and (b) the nonimprinted bis-aniline-cross-linked Au NP composite. All measurements were performed in a 0.1 M HEPES buffer solution (pH = 7.2).

in the electropolymerized Au NP composite. The imprint molecule **2** was washed off from the Au NP composite, and the resulting imprinted matrix was examined for the uptake and release of **2**, while the imprinted and nonimprinted Au NP matrices were compared, and the selectivity features of the **2**-imprinted system were considered. Figure 6A shows the SPR

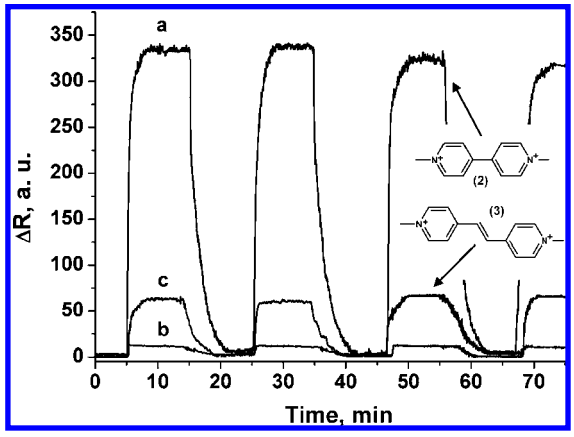

Figure 7. Reflectance changes corresponding to the cyclic electrostimulated uptake and release of (a) MV^{2+} (2 nM) by the MV^{2+}-imprinted bis-aniline-cross-linked Au NP composite-modified Au electrode, (b) MV^{2+} (2 nM) by the nonimprinted bis-aniline-cross-linked Au NP composite, and (c) *N*,*N*′-dimethylbipyridinium-4,4′-ethylene dichloride (2 nM) by the MV^{2+}-imprinted bis-aniline-cross-linked Au NP composite-modified Au electrode. The measurements involved the cyclic application of the reduction, $E = -0.3$ V, and oxidation, $E = 0.4$ V, potential pulses and were performed in a 0.1 M HEPES buffer solution (pH = 7.2).

spectrum of the **2**-imprinted Au NP composite prior to the association of **2** (curve a) and after the equilibration with **2** (1×10^{-6} M) (curve b). The shift in the SPR spectrum indicates the association of **2** to the matrix. Figure 6B depicts the sensograms that correspond to the reflectance changes of the imprinted and nonimprinted Au NP composite systems upon the interaction with variable concentrations of **2** (sensograms I and II, respectively). With the imprinted Au NP system, reflectance changes are observed at a concentration as low as 1×10^{-9} M. The reflectance changes increase as the concentration of **2** is elevated, and they level off to a saturation value at 2×10^{-7} M. For comparison, the nonimprinted Au NP matrix reveals a detectable reflectance change only at a concentration of **2** corresponding to 1×10^{-6} M (Figure 6B, sensogram II). Also, the reflectance changes are minute, indicating a low binding affinity of **2** to the matrix. Furthermore, it should be noted that while the low concentration of **2** in the bulk electrolyte solution (2 nM) does not yield an observable electrochemical response in the presence of the nonimprinted Au NP composite, the uptake of **2** by the **2**-imprinted bis-aniline-cross-linked Au NP composite (bridging units in their reduced, π-donor, state) yields the characteristic electrochemical response of **2** ($E^{o} \sim -0.6$ V vs Ag QRE), due to the local concentration of **2** at the electrode surface. These results clearly demonstrate that upon the electropolymerization of the Au NPs in the presence of **2**, high-affinity imprinted binding sites for **2** were generated. Figure 6C depicts the calibration curves corresponding to the reflectance changes of the imprinted (curve a) and the nonimprinted (curve b) Au NP matrices in the presence of variable concentrations of **2**. The derived association constant of **2** to the imprinted composite was $K_a = 9.0 \times 10^7\ M^{-1}$ (see Supporting Information, Figure S6).

The cyclic, potential-induced uptake and release of MV^{2+} into and from the imprinted and nonimprinted Au NP composites are shown in Figure 7, curves a and b, respectively. The application of the negative potential $E = -0.3$ V on the imprinted matrix results in an increase in the reflectance, consistent with the uptake of **2** into the composite. The application of the positive potential of $E = 0.4$ V leads to a decrease in the reflectance to the base value, implying that **2** is released from the matrix. By the cyclic application of the reductive and oxidative potentials, the reversible uptake and release of **2** are demonstrated, respectively. It should be noted that the nonimprinted Au NP composite shows only low reflectance changes upon interaction with **2** (2×10^{-9} M) and the application of the respective oxidative and reductive potential cycles. These results demonstrate that the nonimprinted Au NP composite neither binds nor releases **2** effectively. Furthermore, the selectivity of the **2**-imprinted Au NP matrix was studied by examining the binding of the structurally related *N*,*N*′-dimethylbipyridinium-4,4′-ethylene dichloride (**3**). Figure 7, curve c, shows the reflectance changes observed upon the application of the reductive and oxidative potentials on the **2**-imprinted composite and its challenging with **3** (2×10^{-9} M). Small reflectance changes are observed, demonstrating the low affinity of **3** for the **2**-imprinted sites and selectivity toward the uptake and release of **2** by the imprinted Au nanoparticle composite (for further selectivity studies, vide infra).

The quantitative analysis of the electrochemically stimulated uptake and release of **2** into and from the (**2**)-imprinted Au NP matrix was examined using Zn(II)−*meso*-tetraphenylsulfonatoporphyrin, Zn(II)−$TPPS^{4-}$, as a diffusional fluorescent probe in the solution. The quenching of Zn(II)−$TPPS^{4-}$ by variable concentrations of (**2**) was examined, and the appropriate calibration curve was extracted (see Supporting Information, Figure S7). The fluorescence spectra of Zn(II)−$TPPS^{4-}$ probe, upon applying the reductive and oxidative potentials on the **2**-imprinted Au NP matrix in the presence of **2** (2×10^{-9} M) are shown in Figure 8A. The application of the reductive pulse, $E = -0.3$ V, results in a higher fluorescence value (curve a), consistent with the uptake of **2** into the matrix. The application of the oxidative potential, $E = 0.4$ V, leads to the oxidation of the bridging units and to a lower fluorescence of the Zn(II)−$TPPS^{4-}$ fluorophore, consistent with the release of **2** from the matrix. The fluorescence differences of Zn(II)−$TPPS^{4-}$ upon the application of the potential cycles are relatively small, yet fully reversible, as depicted in Figure 8B. From the calibration curve that corresponds to the quenching of Zn(II)−$TPPS^{4-}$ by **2** (Figure S7), we conclude that 1.8×10^{-13} mol·cm^{-2} of (**2**) is uptaken and released upon the application of the respective potentials.

As before, we enhanced the uptake and release of **2** from the Au NP composite by the electrosynthesis of the imprinted Au NP matrix on a rough Pt black-modified Au surface. Figure 9A depicts the spectra of Zn(II)−$TPPS^{4-}$ that probes the concentration changes associated with a solution of **2** (2.0×10^{-9} M) that is interacted with the imprinted Au NP composite deposited on the Pt black-modified surface and upon the application of the reductive and oxidative potential pulses on the electrode. At the reductive potential, $E = -0.3$ V, a high fluorescence of Zn(II)−$TPPS^{4-}$ is observed (curve a), consistent with the uptake of **2** from the solution into the composite, resulting in a lower quenching of the chromophore. Upon the application of the oxidative potential on the Au NP sponge, the bis-aniline bridges are oxidized to the quinoid form, a process that releases **2** to the solution. The increase in the concentration of **2** in the solution enhances the quenching of Zn(II)−$TPPS^{4-}$, resulting in a lower fluorescence (Figure 9A, curve b). Continuous cycling of the potentials on the electrode leads to the reversible uptake and release of **2** into and from the Au NP sponge, as evident by the high and low fluorescence intensities of the Zn(II)−$TPPS^{4-}$ (Figure 9B, curve a). For comparison, the fluorescence changes upon the application of the reductive/

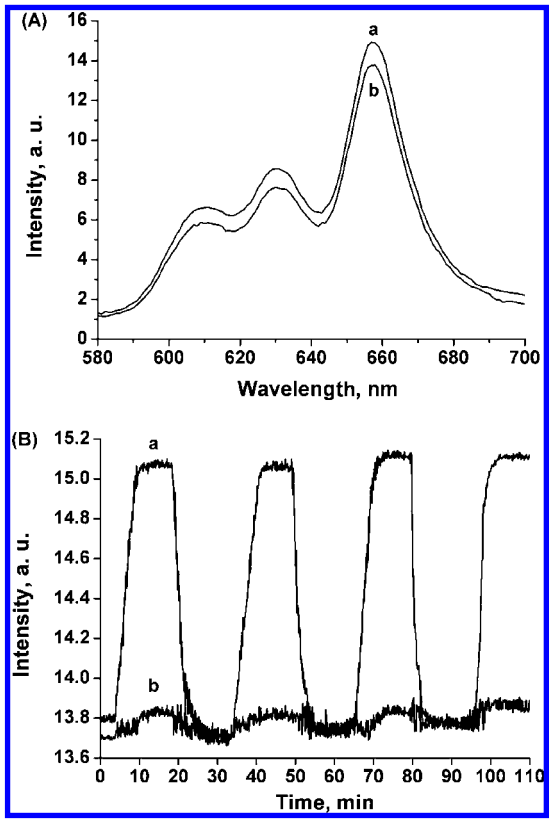

Figure 8. (A) Emission spectra corresponding to Zn(II)−*meso*-tetraphenylsulfonatoporphyrin, Zn(II)−$TPPS^{4-}$ (30 nM), in a 0.1 M HEPES buffer solution (pH = 7.2) that included MV^{2+} (2 nM), following the application of (a) reduction potential, $E = -0.3$ V vs Ag QRE, for 10 min and (b) oxidation potential, $E = 0.4$ V vs Ag QRE, for 10 min on the MV^{2+}-imprinted bis-aniline-cross-linked Au NP composite-modified Au electrode. (B) Switchable fluorescence intensity changes, at $\lambda = 660$ nm, corresponding to Zn(II)−$TPPS^{4-}$ (30 nM), in a 0.1 M HEPES buffer solution (pH = 7.2), following the cyclic electrostimulated uptake and release of MV^{2+} by (a) the MV^{2+}-imprinted bis-aniline-cross-linked Au NP composite-modified Au electrode and (b) the nonimprinted bis-aniline-cross-linked Au NP composite. In all the experiments the concentration of MV^{2+} was 2 nM and the excitation wavelength was $\lambda_{ex} = 445$ nm.

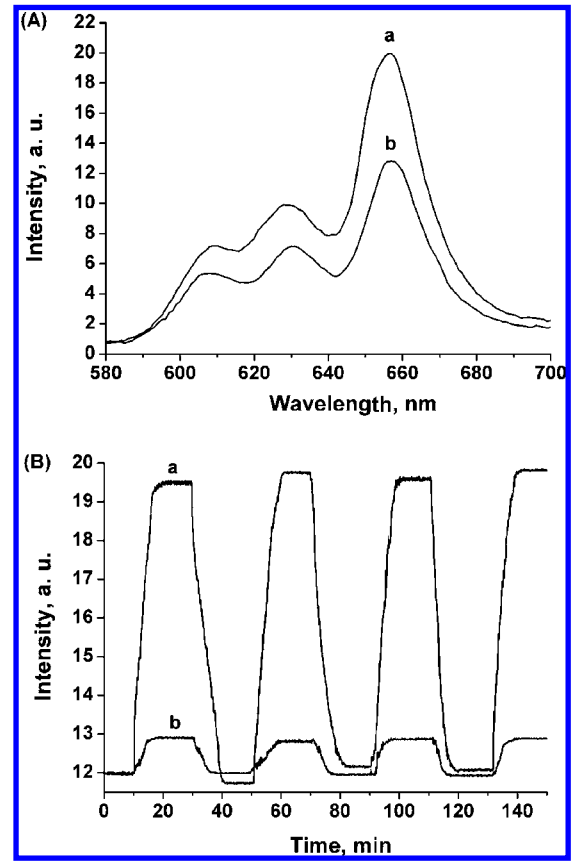

Figure 9. (A) Emission spectra corresponding to the Zn(II)−*meso*-tetraphenylsulfonatoporphyrin, Zn(II)−$TPPS^{4-}$, 30 nM, in a 0.1 M HEPES buffer solution (pH = 7.2) that included MV^{2+} 2 nM, following the application of (a) reduction potential, $E = -0.3$ V vs Ag QRE, for 10 min and (b) oxidation potential, $E = 0.4$ V vs Ag QRE, for 10 min on the MV^{2+}-imprinted bis-aniline-cross-linked Au NP composite-modified Pt black-roughened Au electrode. (B) Switchable fluorescence intensity changes, at $\lambda = 660$ nm, corresponding to Zn(II)−$TPPS^{4-}$ (30 nM) in a 0.1 M HEPES buffer solution (pH = 7.2), following the cyclic electrostimulated uptake and release of MV^{2+} by (a) the MV^{2+}-imprinted bis-aniline-cross-linked Au NP composite-modified Pt black-roughened Au electrode and (b) the nonimprinted bis-aniline-cross-linked Au NP composite-modified Pt black-roughened Au electrode. In all the experiments the concentration of MV^{2+} was 2 nM and the excitation wavelength was $\lambda_{ex} = 445$.

oxidative potential cycles on the nonimprinted Au NP composite on the rough Pt black-deposited Au surface are depicted in Figure 9B, curve b. The small fluorescence changes indicate the inefficient uptake and release of **2** by the nonimprinted matrix. By following the fluorescence changes of Zn(II)−$TPPS^{4-}$ and using the corresponding calibration curve (Figure S7, Supporting Information), we find that 7.1×10^{-13} mol·cm^{-2} of **2** binds to the **2**-imprinted Au NP sponge upon the application of the reductive potential, $E = -0.3$ V, and this amount is released from the sponge upon the application of the oxidative potential, $E = 0.4$ V.

A further aspect to consider relates to the amounts of picric acid (**1**) and *N*,*N*′-dimethyl-4,4′-bipyridinium (**2**) uptaken and released by the respective imprinted matrices. One may realize that the association constant for the binding of picric acid (**1**) to its imprinted sites is higher than the binding constant of **2** to its imprinted sites ($K_a^{\mathbf{1}} = 3.9 \times 10^{12}$ M^{-1} vs $K_a^{\mathbf{2}} = 9.0 \times 10^{7}$ M^{-1}). The amount of **2** uptaken and released by the **2**-imprinted Au NP composite is, however, 2.5-fold higher than that uptaken/released by the **1**-imprinted composite. This apparent discrepancy is explained by the fact that the electropolymerization of the functionalized Au NPs in the presence of the cationic **2** is substantially more efficient than the electropolymerization in the presence of **1**. Coulometric analysis of the redox response of the bis-aniline bridges cross-linking the Au NP composites generated by 60 electropolymerization cycles, in the presence of **1** or **2**, reveals that the charge associated with the redox response of the bridging units formed in the presence of **2** is ca. 3-fold higher than that observed for the **1**-imprinted composite. That is, the electrosynthesis of the **2**-imprinted matrix led to more imprinted sites as compared to the **1**-imprinted Au NP composite. The enhanced efficiency for the formation of the **2**-imprinted matrix is consistent with previous reports[19] demonstrating that the electropolymerization of aniline units in the presence of cationic substrates is highly efficient.

The selectivity of the imprinted recognition sites in the Au NP sponge was further demonstrated by imprinting *N*,*N*′-

(19) (a) Zotti, G.; Catterin, S.; Comisso, N. *J. Electroanal. Chem.* **1988**, *239*, 387–395. (b) Kazarinov, V. E.; Andreev, V. N.; Spytsin, M. A.; Shlepakov, A. V. *Electrochim. Acta* **1990**, *35*, 899–904. (c) Desilvestro, J.; Scheifele, W. *J. Mater. Chem.* **1993**, *3*, 263–272. (d) Tang, H.; Kitani, A.; Shiotani, M. *Electrochim. Acta* **1996**, *41*, 1561–1567. (e) Okamoto, H.; Kotaka, A. *Polymer* **1999**, *40*, 407–417.

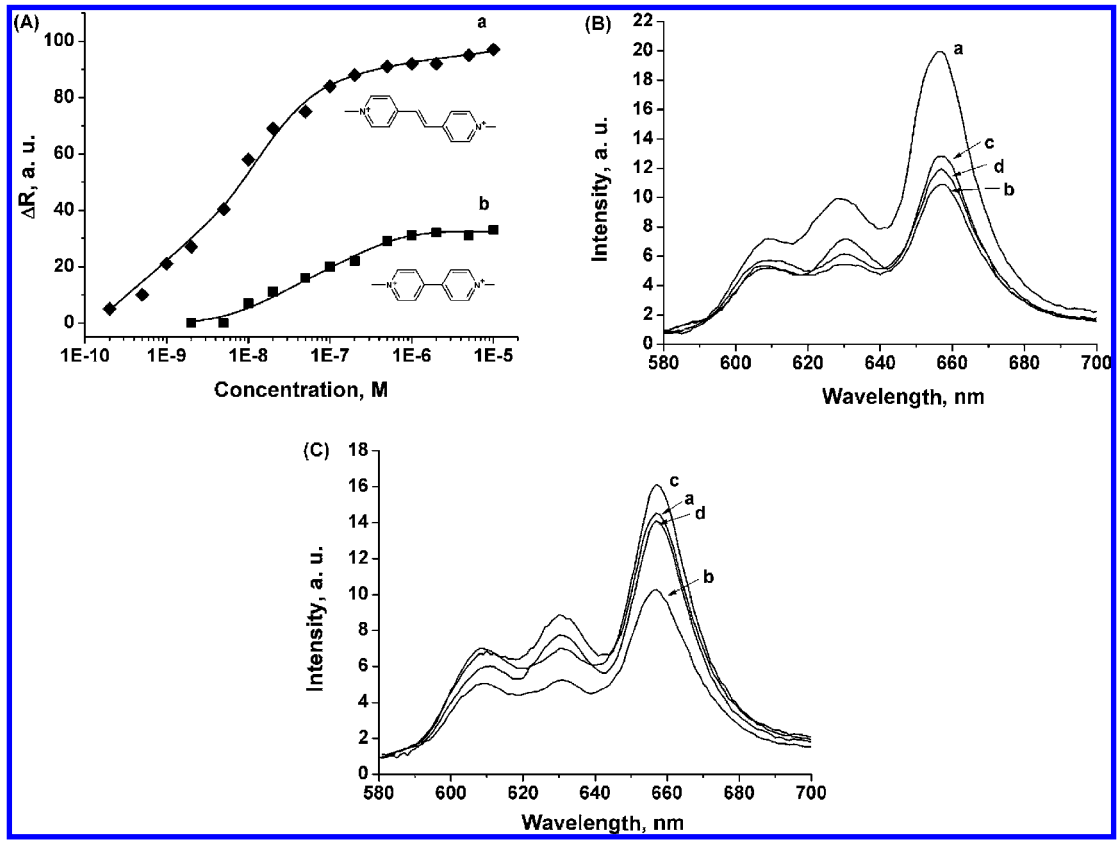

Figure 10. (A) Calibration curves corresponding to the reflectance changes at the *N*,*N*′-dimethylbipyridinium-4,4′-ethylene dichloride (**3**)-imprinted bis-aniline-cross-linked Au NP composite-modified Pt black-roughened Au electrode upon the analysis of different concentrations of (a) *N*,*N*′-dimethylbipyridinium-4,4′-ethylene dichloride (**3**) and (b) *N*,*N*′-dimethyl-4,4′-bipyridinium dichloride (**2**). All measurements were performed in a 0.1 M HEPES buffer solution (pH = 7.2). (B) Emission spectra corresponding to the Zn(II)−*meso*-tetraphenylsulfonatoporphyrin, Zn(II)−$TPPS^{4-}$ (30 nM) in a 0.1 M HEPES buffer solution (pH = 7.2) in the presence of the **2**-imprinted bis-aniline-cross-linked Au NP composite-modified Pt black-roughened Au electrode, following the application of (a) $E = -0.3$ V vs Ag QRE in the presence of **2** (2 nM), (b) $E = 0.4$ V vs Ag QRE in the presence of **2** (2 nM), (c) $E = -0.3$ V vs Ag QRE in the presence of **3** (2 nM), and (d) $E = 0.4$ V vs Ag QRE in the presence of **3** (2 nM). (C) Emission spectra corresponding to the Zn(II)−*meso*-tetraphenylsulfonatoporphyrin, Zn(II)−$TPPS^{4-}$ (30 nM) in a 0.1 M HEPES buffer solution (pH = 7.2) in the presence of the **3**-imprinted bis-aniline-cross-linked Au NP composite-modified Pt black-roughened Au electrode, following the application of (a) $E = -0.3$ V vs Ag QRE in the presence of **3** (2 nM), (b) $E = 0.4$ V vs Ag QRE in the presence of **3** (2 nM), (c) $E = -0.3$ V vs Ag QRE in the presence of **2** (2 nM), and (d) $E = 0.4$ V vs Ag QRE in the presence of **2** (2 nM). In all experiments the duration of the applied potential pulses was 10 min.

dimethylbipyridinium ethylene (**3**) into the matrix and studying its uptake and release in comparison to the uptake/release of **2** by the **3**-imprinted sponge. Figure 10A, curve a, shows the reflectance changes observed upon analyzing different concentrations of **3** by the **3**-imprinted Au NP composite. From the curve, we derived the association constant of **3** to the matrix, $K_a^3 = 1.6 \times 10^8$ M^{-1}. As before, the nonimprinted Au NP composite yields negligible reflectance changes upon interaction with **3**. The **3**-imprinted Au NP matrix was, then, challenged with *N*,*N*′-dimethyl-4,4′-bipyridinium (**2**) (Figure 10A, curve b). Substantially lower reflectance changes are observed, implying that **2** has a lower affinity for the association to the **3**-imprinted Au NP composite and that selectivity was, indeed, obtained. Furthermore, it should be noted that the **2**- or **3**-imprinted bis-aniline-cross-linked Au NP composites did not reveal any significant affinity toward picric acid (similar responses as the nonimprinted composites). This further emphasizes the significance of the imprinting procedure in the preparation of selective imprinted matrices.

The selective quantitative uptake and release of **2** and **3** to and from the respective **2**- and **3**-imprinted sponges were demonstrated by fluorescence studies using Zn(II)−$TPPS^{4-}$ as a reporter. Figure 10B, curves a and b, show the fluorescence intensities of the fluorophore upon interaction of the Pt black-roughened **2**-imprinted Au NPs with **2**, at the applied potentials of $E = -0.3$ V and $E = 0.4$ V, respectively. The high and low fluorescence intensities correspond to the uptake and release of **2** by the **2**-imprinted sponge. For comparison, curves c and d show the fluorescence intensities generated by the **2**-imprinted sponge upon interaction with **3**, and applying the same potential pulses. Again, high and low fluorescence intensities are, respectively, observed. The difference between the high and low fluorescence values for **2** is, however, substantially higher than those observed for **3**, implying more efficient uptake and release of **2** as compared to **3**. Using the calibration curve that corresponds to the quenching of Zn(II)−$TPPS^{4-}$ by **3** (Figure S8, Supporting Information), we find that the amount of **3** uptaken and released by the **2**-imprinted sponge is 1.8×10^{-13} mol·cm^{-2}, 4-fold lower than the content of **2** bound and released by the same matrix. The results are reversed upon the interaction of the **3**-imprinted Au NP composite with **2** or **3**, while the different potentials were applied (Figure 10C). Using the appropriate calibration curves, we conclude that 5.6×10^{-13} mol·cm^{-2} of **3** are uptaken and released by the **3**-imprinted matrix, while only 2.5×10^{-13} mol·cm^{-2} of **2** are bound and released by the **3**-imprinted composite. These results clearly demonstrate that the imprinting procedure led

to selective uptake/release of the substrates by the respectively imprinted Au NP sponges.

Conclusions

The present study has introduced the use of imprinted bis-aniline-cross-linked Au NP composites on electrodes as electrochemically triggered sponges for the uptake and release of substrates. Specifically, we demonstrated that the electrochemically controlled reduction and oxidation of the bis-aniline cross-linking units control the π-donor−acceptor interactions between the bridges and the π-acceptor substrates. This enabled the electrochemically stimulated uptake and release of the π-acceptor substrates by the Au NP matrix. We further demonstrated that the imprinting of molecular recognition sites in the cross-linked Au NP composite yielded specific NP sponges exhibiting high-capacity uptake of the π-acceptor substrates. We believe that the electrified Au NPs sponges hold promise for future nanotechnology applications, such as drug delivery or removal of environmental pollutants (for example, the removal of the MV^{2+} herbicide or nitroaromatics from contaminated soil).

Experimental Section

Chemicals and Instrumentation. Ultrapure water from NANOpure Diamond (Barnstead) source was used in all of the experiments. Picric acid and *N*,*N*′-dimethylbipyridinium-4,4′ dichloride (MV^{2+}) were obtained from Sigma-Aldrich. *meso*-Tetramethylpyridinium porphyrin, $TMPyP^{4+}$, was obtained from Aldrich and the *meso*-tetraphenylsulfonatoporphyrin, $TPPS^{4-}$, was obtained from Strem Chemicals, Inc. Zn(II)−$TPPS^{4-}$ was synthesized by boiling $TPPS^{4-}$ with $ZnCl_2$ in an aqueous solution for 3 h.

Synthesis of Nanoparticles. Au nanoparticles functionalized with 2-mercaptoethanesulfonic acid and *p*-aminothiophenol (Au NPs) were prepared by mixing a 10 mL solution containing 197 mg of $HAuCl_4$ in ethanol and a 5 mL solution containing 42 mg of mercaptoethanesulfonate and 8 mg of *p*-aminothiophenol in methanol. The two solutions were stirred in the presence of 2.5 mL of glacial acetic acid in an ice bath for 1 h. Subsequently, 7.5 mL of aqueous solution of 1 M sodium borhydride ($NaBH_4$) was added dropwise, resulting in a dark-colored solution associated with the presence of the Au NPs. The solution was stirred for an additional hour in an ice bath and then for 14 h at room temperature. The particles were successively washed and centrifuged (twice in each solvent) with methanol, ethanol, and diethyl ether. A mean particle size of ca. 4.0 nm was estimated using TEM.

Chemical Modification of the Electrodes. *p*-Aminothiophenol-functionalized electrodes were prepared by immersing the Au slides for 24 h into a *p*-aminothiophenol ethanolic solution (50 mM). In order to prepare the bis-aniline-cross-linked Au NP composite on the electrode, the surface-tethered *p*-aminothiophenol groups were electropolymerized in a 0.1 M HEPES buffer solution (pH = 7.2) containing 1 mg·mL^{-1} of *p*-aminothiophenol-functionalized Au NPs. The polymerization was performed by the application of 10 potential cycles between $E = -0.35$ and $E = 0.8$ V vs a Ag wire quasireference electrode, at a potential scan rate of 100 mV s^{-1}, followed by applying a fixed potential of $E = 0.8$ V for 30 min. The resulting films were then washed with the background buffer solution to exclude any residual monomer from the electrode. Similarly, imprinted bis-aniline-cross-linked films were prepared by adding 1 mg·mL^{-1} of the imprint molecule to the Au NPs mixture prior to the electropolymerization process. The extraction of the picric acid from the film was carried out by immersing the electrodes in a 0.1 M HEPES solution, pH = 7.2, for 2 h at room temperature. The full removal of imprint molecules from the electropolymerized film was verified by the SPR curve shifts. Pt black roughening was performed by immersing the Au slides in a 0.5 M H_2SO_4 solution containing 5 mM K_2PtCl_6 and applying a constant potential of $E = -0.75$ V vs a Pt wire QRE for 2 min.

Fluorescence Assay of the Uptake and Release Processes. The imprinted Au NPs matrices were subjected to electrolyte solutions that included the respective substrates (**1**−**3**) and the respective fluorophores. The fluorescence changes of the fluorophores were monitored upon the application of a reduction potential (for the uptake of the substrates) or an oxidation potential (for the release of the substrates). The concentrations of the respective substrates in the different experiments were selected in such a way that they corresponded to the lowest values that led to significant quenching of the respective fluorophores. It should be noted that the fluorescence spectra of the different fluorophores in the electrolyte solutions were unaffected, in the absence of the substrates, by the presence of the Au NP composites or by the potentials applied on the composites. Fluorescence measurements were performed using a Cary Eclipse Device (Varian Inc.). For these measurements a Au wire electrode (working area 0.4 cm^2) and a 200 μL cuvette were used.

Surface Plasmon Resonance (SPR) Analysis of the Uptake and Release Processes. A surface plasmon resonance (SPR) Kretschmann-type spectrometer NanoSPR 321 (NanoSPR devices) with a LED light source, $\lambda = 650$ nm, and with a prism refraction index of $n = 1.61$ was used in this work. Au-coated semitransparent glass slides (Mivitec GmbH, Analytical μ-Systems) were used for the SPR measurements. A home-built Perspex cell equipped with a Pt auxiliary electrode (0.5 mm diameter wire) and a Ag wire quasireference electrode (0.5 mm diameter wire) was mounted on the Au surfaces functionalized with the bis-aniline-cross-linked Au NP composites (imprinted or nonimprinted), acting as the working electrode and the SPR support. The respective substrates **1**−**3** were injected into the electrolyte solution to yield the specified concentrations. Full SPR spectra or at a single incident angle (sensograms) were recorded for the different systems, while a reductive potential corresponding to $E = -0.3$ V vs Ag QRE (to yield the bis-aniline π-donor sites) or an oxidative potential of $E = 0.4$ V vs Ag QRE (to yield the quinoid π-acceptor groups) were applied. For these measurements, an Autolab electrochemical system (Echo Chemie, The Netherlands) driven by GPES software was used.

Acknowledgment. This research is supported by the EU ECCell project.

Supporting Information Available: SPR curves recorded for the Au NPs matrices before and after the imprinting and the extraction of the picric acid and methyl viologen molecules, a cyclic voltammetry of the bis-aniline-cross-linked Au NP composite-modified Au electrode, Langmuir plots for the evaluation of the association constants of picric acid and methyl viologen to the respectively imprinted Au NPs matrices, and the emission spectra of the $TMPyP^{4+}$ and Zn(II)−$TPPS^{4-}$ in the presence of picric acid and methyl viologen, respectively. This material is available free of charge via the Internet at http://pubs.acs.org.

JA102153F